Physics of the Earth and Planetary Interiors, 18 (1979) 197–208

THE KALAPANA EARTHQUAKE OF NOVEMBER 29, 1975: AN INTRA-PLATE EARTHQUAKE AND ITS RELATION TO GEOTHERMAL PROCESSES [1]

AUGUSTINE S. FURUMOTO and ROBERT L. KOVACH [2]

Hawaii Institute of Geophysics, Honolulu, HI 96822 (U.S.A.)

(Received February 21, 1978; accepted for publication May 16, 1978)

Furumoto, A.S. and Kovach, R.L., 1979. The Kalapana earthquake of November 29, 1975: an intra-plate earthquake and its relation to geothermal processes. Phys. Earth. Planet. Inter., 18: 197–208.

By use of teleseismic and local data, the P-wave source mechanism of the Kalapana, Hawaii, earthquake of November 29, 1975 was found to have a common strike of N64°E for the two nodal planes. One plane dipped 4° to the NW; the other dipped 86° to the SE. After consulting subsurface geological data obtained by the recent Hawaii geothermal exploration program, it was decided that the plane dipping to the NW at 4° was the preferred solution.

Seismic moment obtained from body-wave data and surface-wave data averaged $1.2 \cdot 10^{27}$ dyn cm. Fault area from P-wave, surface wave and tsunami data amounted to about 2200 km^2. Stress drop was on the order of tens of bars.

The earthquake appears to be of volcanic origin. When magma pressure in the dike complex of the east rift of Kilauea exceeded the fracture point, the southern flank of the east rift was pushed across the ancient sea floor upon which the volcanic edifice rests. The result was a low-angle overthrust, which also produced a tsunami. The hypothesis of forceful intrusion of magma into the east rift is consistent with the mechanism of the earthquake.

The low stress drop (in relation to other intra-plate earthquakes) is probably due to the occurrence of the earthquake in a hot-rock regime.

1. Introduction

During the early morning hours of November 29, 1975, an earthquake of magnitude 7.2 rocked the SE part of the island of Hawaii known as the Puna District, and generated a tsunami that killed two persons and caused extensive damage to buildings. Because the Puna District was sparsely populated, the damage in terms of dollars was in the range of one or two million, a relatively small amount for such a large eartquake. The two persons who died were campers who were trapped on an isolated beach.

[1] Hawaii Institute of Geophysics contribution No. 924.
[2] On leave from Stanford University, Stanford, CA 94305, U.S.A.

The epicenter of the earthquake was located at 19°20′06″N, 155°01′45″W, at a depth of 7 km, according to determinations by the staff of the Hawaiian Volcano Observatory at Kilauea, Hawaii. The origin time was November 29, 1975 at $14^h47^m42^s$ (GMT), which was 04^h47^m local time.

Because the earthquake generated a local tsunami that was the second largest in recorded history, a project was undertaken to investigate the generating mechanism. In the course of the investigation, it became apparent that the earthquake was closely associated with magmatic processes along the east rift of Kilauea volcano. This paper presents our results concerning the earthquake source mechanism and its relation to geothermal processes.

2. Source mechanism by P waves

Full-size copies of seismograms from 25 worldwide stations were obtained from the World Data Center. Preliminary examination of the seismograms revealed that for many stations, the first arrivals were weak. The reason, we later found, was that these stations were close to a nodal plane. To overcome this difficulty, the epicentral distances to various stations were first calculated and the expected arrival times for each station were determined by using the *Travel Time Tables* of Herrin et al. (1968). Then the polarities were measured at the expected arrival time in the seismograms. Because the earthquake was a large one, the initial P wave usually had a period in the range of 6–8 s on the long-period seismograms. A deviation of 2 s one way or the other in the expected travel time did not lessen the chance of phases being read correctly. In this approach, the travel time as determined was very reliable, because the focus was very precisely determined by a local seismograph network on the island of Hawaii.

Data concerning the stations that were used are listed in Table I. The coordinates of the stations were omitted as these can be readily found in publications from the World Data Center. The expected arrival times for the various stations are published here to aid those who may want to verify the data as we have obtained them.

A plot of the compressions and dilatations on a Wulff-net bottom-hemisphere projection is shown in Fig. 1. The only nodal plane determinable has a strike of N64°E and a dip of 86°. Because several stations were clustered around the nodal plane, the plane was determinable to 0.5° precision without the use of statistical means.

In addition to teleseismic data, we examined seismograms from the network of stations on the island of Hawaii maintained by the Hawaiian Volcano Observatory of the USGS. A plot of the distribution of

TABLE I

Teleseismic P-wave data for source mechanism determinations

Station	Epicentral distance (deg)	Azimuth (deg)	Travel time (^{m} s)	Arrival time (^{h} m s)	Signature	I_h * (deg)
HKC	83.48	291.4	12 30.4	14 00 12	C	17.0
GIE	66.0	98.13	10 46	14 58 28	D	22.0
ANP	76.2	292.2	11 48	14 59 30	C	19.1
COL	45.8	4.3	8 23	14 56 05	C	27.2
TAU	83.5	216.3	12 28	15 00 10	D	17.1
SBA	99.7	187.6	13 45	15 01 27	D	15.4
LON	38.6	37.0	7 22	14 55 04	C	28.8
BHP	73.4	86.1	11 31	14 59 13	D	19.8
KIP	3.5	307.2			C	54.7
BAG	79.5	283.9	12 07	14 59 49	C	18.2
GUA	57.6	274.1	9 50	14 57 32	C	24.3
DAV	77.7	273.3	11 58	14 59 40	C	18.7
ADE	83.0	229.1	12 25	15 00 07	D	17.2
RIV	73.8	224.3	11 34	14 59 16	D	19.7
RAB	57.0	251.32	9 45	14 57 27	D	24.0
LPS	62.9	83.4	10 26	14 58 08	D	22.5
SPA	109.335	180	18 31	15 06 13	D	8.0
CTA	69.8	238.8	11 10.4	14 58 53	C	20.9
LEM	99.17	265.9	13 41	15 01 23	C	15.4
PMG	63.8	248.54	10 32	14 58 14	C	22.3
MUN	99.10	239.2	13 42	15 01 24	C	15.4
CHG	98.0	293.2	13 36	15 01 18	D	15.4
MAT	60.25	301.8	10 08	14 57 50	C	23.2
BKS	34.0	49.9	6 43.5	14 54 25.5	C	29.9

* the angles of incidence I_h were obtained from tables by Pho and Behe (1972).

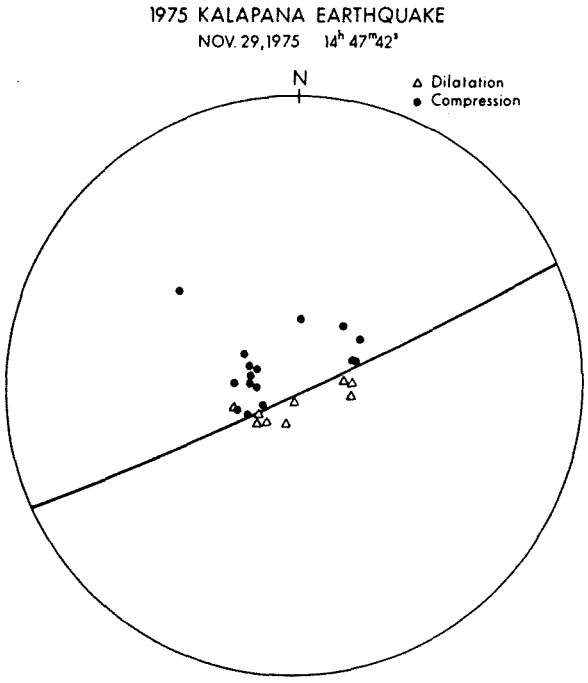

Fig. 1. Fault-plane solution of the Kalapana earthquake of November 29, 1975 from teleseismic data. The nodal plane strikes N64°E and dips 86°.

the compressions and dilatations for the various stations is shown in Fig. 2. The base map showing topographic contours, volcanic centers and rift zones was provided by Macdonald (1956). The epicenter of the earthquake is shown by a cross. The straight line through the epicenter is the strike of the nodal plane as determined by teleseismic data of Fig. 1. The circle represents a distance of 62.0 km from the epicenter.

The distance of 62 km was found to be the boundary between dilatations and compressions when a plot of arrival times against epicentral distances was drawn (Fig. 3). In the construction of the plot, elevation corrections were included. The lone dilatation beyond 62 km is that of the South Point station (18° 53.9′N, 155°39.9′W), which according to Fig. 2 is in a quadrant that should be dilatation.

Another significant factor in Fig. 3 is that the early dilatations define a velocity of 7.1 km/s, the same value obtained by Hill (1969) from seismic refraction studies for the lower crustal layer under the island. The focal depth of 7 km puts the focus of the earthquake at the top of the 7.1-km/s layer defined by Hill. Also, Hill's data showed that the mantle velocity under the islands is 8.2 km/s. From Fig. 3 it is evident that dilatations were observed at those stations where the ray path was limited to the 7.1-km/s layer and shallower layers, but the compressions were recorded when the ray paths included the mantle. The mantle velocity is not discernible in the later arrivals because the arrival times are scattered. The scatter shows that the Mohorovicic discontinuity under the island has large undulations.

As seen in Fig. 2, the nodal line from teleseismic data is consistent with the local distribution of signatures. Near the epicenter a compression is located right on the nodal line, and there is a dilatation just to the north of the nodal line a short distance away. These distributions do not allow much flexibility to the orientation of the nodal line; the 62-km arc also is rather inflexible, as seen from the distribution of compression and dilatation near the summit of Mauna Loa.

Strictly speaking, the second nodal plane is indeterminant from both the teleseismic and local data we have presented so far, but we can place some constraints on its orientation. It is evident that the second nodal plane dips to the NW and has a dip angle less than 30°. This value was inferred from the fact that dilatations to the NW were confined to travel paths in the 7.1-km/s layer, while the compressions included mantle paths. Since the critical angle of incidence at an interface of 7.1 and 8.2 km/s is 60°, the nodal plane separating dilatations and compressions must have a dip less than 30°. Another constraint is that the second nodal plane must be orthogonal to the first nodal plane.

From the distribution of signatures in Fig. 2, we can say that the strike of the second nodal plane is almost the same as the strike of the teleseismic or first nodal plane, differing at most by a few degrees, if at all. The teleseismic data of Fig. 1 and the local data of Fig. 2 preclude the drawing of a nodal plane that has a significant strike-slip component. The solution is then an overthrust mechanism. To obtain a simplified solution, the strike of the second nodal plane was taken to coincide with the strike of the teleseismic nodal plane. Then the second nodal plane would have a 4° dip in the direction of azimuth 334°, or an updip of 4° in the 154° direction.

A diagrammatic representation of the double-couple solution is shown in Fig. 4. Of the two nodal

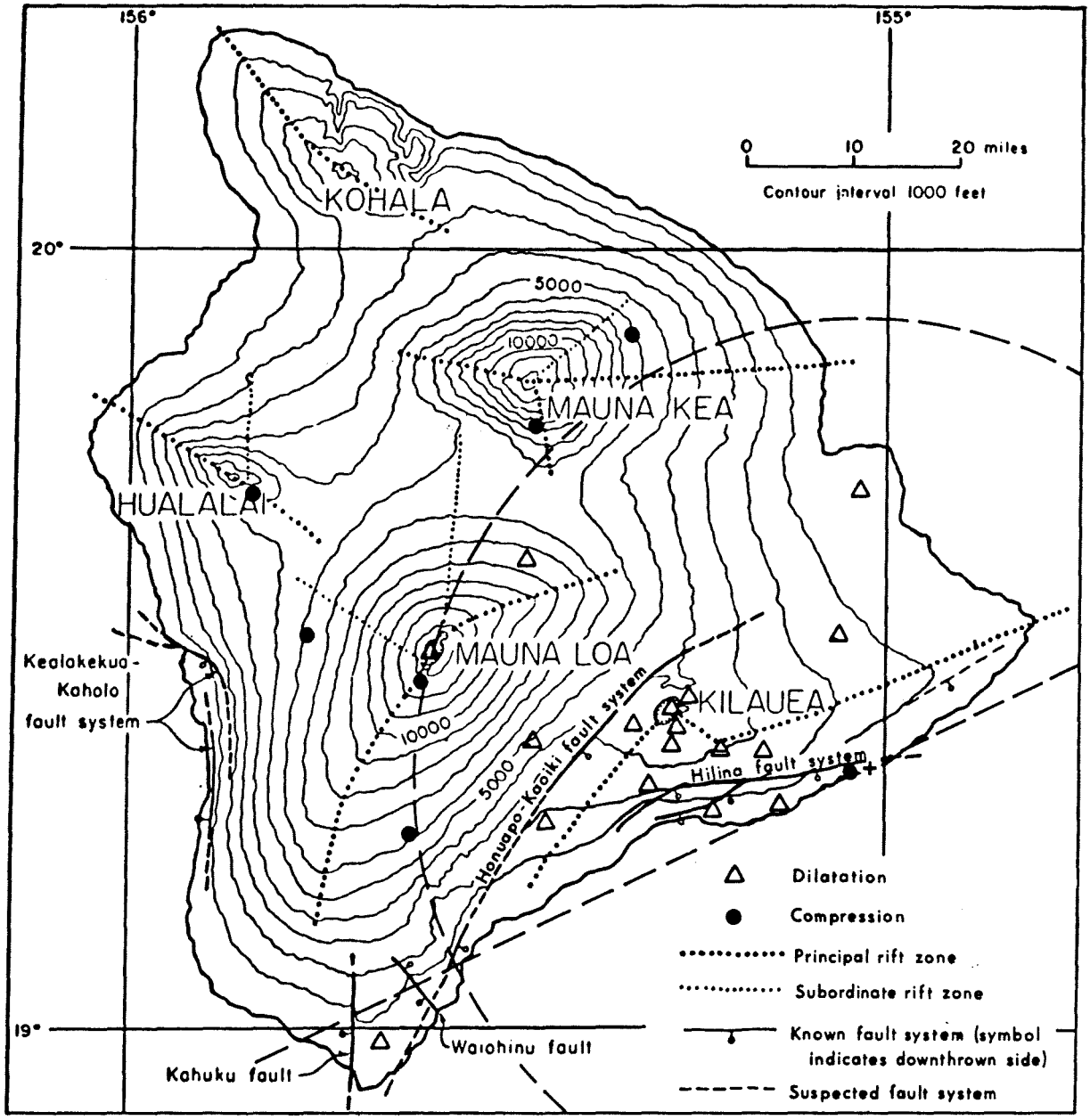

Fig. 2. Distribution of dilatations and compressions recorded by local network of seismic stations maintained by Hawaiian Volcano Observatory. The N64°E-striking line is the nodal plane by teleseismic data. The 62-km radius neatly divides the signatures into compressions and dilatations.

planes T and L, the low-angle overthrust across plane L from the NW to the SE was chosen as the preferred solution after examination of recent geological data. Since 1973 a coordinated exploration program involving diverse types of geophysical surveys has been carried out over the Puna District in search of geothermal resources (Furumoto, 1976; Furumoto and Broyles, 1977). In all the voluminous seismic, gravity and mag-

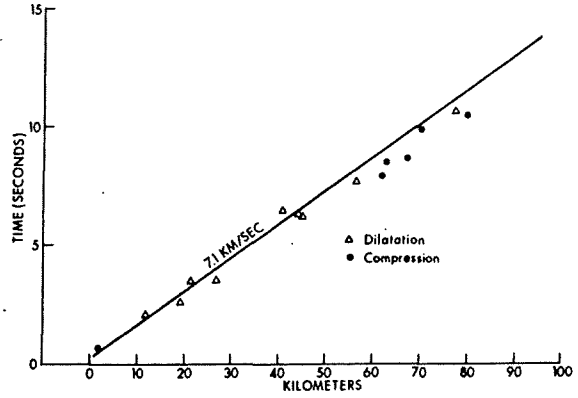

Fig. 3. Travel-time plot of Kalapana earthquake P-wave arrivals. The arrival times are relative, as time correction on multichannel recorder was not obtained. Triangles indicate dilatations and dots indicate compressions. Elevation corrections were included.

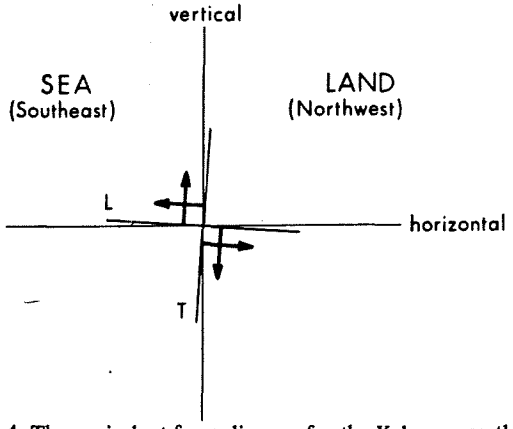

Fig. 4. The equivalent force diagram for the Kalapana earthquake. The plane strikes along azimuth 154°. The nodal planes are 4° from vertical and horizontal axes.

netic data collected, there has been no evidence of an overthrust fault oriented as plane *T*, but there was much evidence in support of plane *L* as the fault plane.

3. Seismic moment from body-wave data

Seismic moment and stress drop for the earthquake were determined by use of both P- and S-wave data. Seismograms from Guam (*GUA*) and Rabaul (*RAB*), and from Balboa Heights (*BHP*) and Tasmania University (*TAU*) were used for P- and S-wave data, respectively. These seismograms were chosen because of their legibility.

For digitizing and analyzing, the techniques of Hanks and Wyss (1972), and for travel-path distances and for attenuation, the results of Julian and Anderson (1968) were consulted. For obtaining the spectral level of S waves, exactly the same data windows were used for EW and NS seismograms, and the spectra of

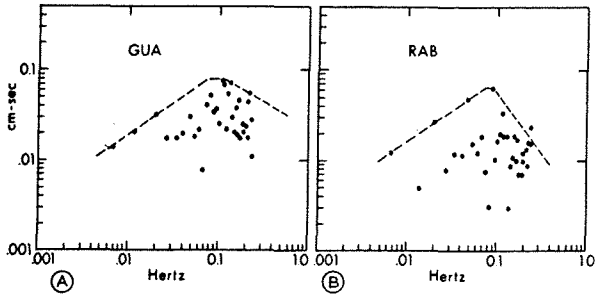

Fig. 5. P-wave spectra from stations *GUA* (A) and *RAB* (B).

TABLE II

Seismic moment by body waves

Station	Δ (deg)	Spectral level (cm s)	Corner frequency (Hz)	Seismic moment (10^{27} dyn cm)	Fault radius (km)	Stress drop (bar)
P-waves:						
GUA	57.6	0.079	0.12	1.2	22	49
RAB	57.0	0.063	0.09	1.1	29	21
S-waves:						
BHP	86.1	0.58	0.017	1.8	83	1.4
TAU	83.5	0.68	0.025	1.2	57	2.8

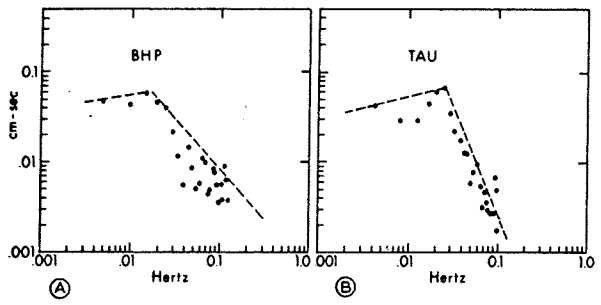

Fig. 6. S-wave spectra from stations *BHP* (A) and *TAU* (B).

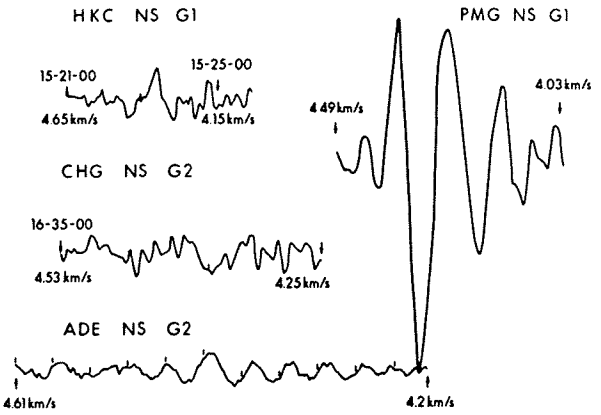

Fig. 7. Samples of G_1 and G_2 recordings used in surface wave analysis.

the two components were added vectorially. In the *TAU* seismograms, as the SKS phase came in toward the end of the S phase, the data window included both the S and SKS phases.

The P-wave spectra from *GUA* and *RAB* are shown in Fig. 5; the S-wave spectra from *BHP* and *TAU* are given in Fig. 6. From these diagrams, the spectral level and corner frequencies can be easily read. The values used for seismic moment calculations were: density, 2.7 g/cm^3; P-wave velocity, 7.1 km/s; S-wave velocity, 3.8 km/s. To derive the S-wave velocity from the P-wave velocity, a Poisson's ratio of 0.3 was used; this value was observed for the area including the epicenter by Keller (1975). The directional functions were calculated for the preferred orientation of the source mechanism as derived in the previous section. The formulas used for calculations are those quoted by Hanks and Wyss (1972). The results of the calculations are given in Table II.

The seismic moment, whether determined by P- or S-wave, was in the neighborhood of $1.3 \cdot 10^{27}$ dyn cm, a value that agrees with Ando's (1976). The fault radii obtained by S-wave data are larger by factors of 2 to 4 than those obtained by P-wave data.

From P-wave data, the fault area would be about 2600 km^2; from S-wave data, 22,000 or 10,000 km^2. From tsunami data, Hatori (1976) estimated the rupture area to be about 2200 km^2. P-wave data calculations are most consistent with tsunami data.

S-wave data gave stress drops of only a few bars, but P-wave data results were 20 and 49 bar. The P-wave values are more consistent with surface wave stress drops as obtained in the next section.

4. Seismic moment from surface-wave data

The Kalapana earthquake also generated clear G_1 and G_2 surface waves recorded on the long-period seismographs of many worldwide stations. Some typical G_1 and G_2 signals are shown in Fig. 7. We can also examine the compatibility of the observed spectral amplitudes for the G_1 and G_2 waves with our preferred fault-plane solution utilizing the amplitude equalization technique discussed by Ben-Menahem and Harkrider (1964) and Harkrider (1970).

In our calculations, the standard coordinate geometry is adopted with the fault at a depth $z = h$, striking in the positive X-direction and having a dip angle δ associated with the footwall. The displacement vector indicates motion of the hanging wall and is specified by a slip angle λ measured counterclockwise from a horizontal line parallel to the strike. The position of the recording station is given by the coordinates $\theta, r, z = 0$ where r is the epicentral distance and θ is measured counterclockwise from the positive X-direction.

For a double-couple source, equivalent to a slip dislocation along a fault, the spectral amplitude of displacement due to Love waves observed at a station is given by:

$$U = S\left(\frac{2\pi}{cTr}\right)^{1/2} A\chi(\theta, h) \exp[-i(kr + 3\pi/4)]$$

where S = spectral source-time function, c = phase velocity, T = period, A = Love wave amplitude

TABLE III

Amplitude equalization of 100-s Love waves

Station	Observations					Corrections				Results
	spectral ground motion (cm s)	wave	compo-nent	azi-muth (deg)	Δ (km)	$(\sin \Delta/a)^{1/2}$	$\exp \gamma_L(\Delta-10{,}000)$ (1)	$1/sc\varphi$ (2)	spectral ground motion (3), flat earth at $\Delta = 90^\circ$	Moment (10^{26} dyn cm)
Guam (*GUA*)	0.465	G_1	NS	274.1	6,417	0.919	0.71	1.03	0.249	6.8
Guam (*GUA*)	0.053	G_2	NS	274.1	33,613	0.919	5.22	1.03	0.209	5.7
Hong Kong (*HKC*)	0.244	G_1	NS	291.3	9,297	0.997	0.94	1.05	0.192	4.7
Hong Kong (*HKC*)	0.072	G_2	NS	291.3	30,733	0.997	4.27	1.05	0.257	6.3
Davao (*DAV*)	0.152	G_1	NS	273.3	8,649	0.988	0.88	1.05	0.111	3.2
Baguio (*BAG*)	0.113	G_2	NS	283.8	31,176	0.991	4.40	1.05	0.413	10.1
College (*COL*)	0.378	G_1	EW	4.3	5,090	0.846	0.63	1.01	0.162	4.7
College (*COL*)	0.064	G_2	EW	4.3	34,941	0.846	5.73	1.01	0.250	7.1
Anpu (*ANP*)	0.196	G_1	NS	292.0	8,488	0.985	0.87	1.04	0.139	3.5
Lembang (*LEM*)	0.247	G_1	NS	265.9	11,036	0.993	1.10	1.05	0.226	7.5
Tasmania University (*TAU*)	0.108	G_2	NS	219.0	30,962	0.995	4.34	1.24	0.461	13.9
Balboa Heights (*BHP*)	0.211	G_1	NS	86.1	8,137	0.978	0.84	1.05	0.145	4.8
Port Moresby (*PMG*)	0.320	G_1	NS	268.7	6,305	0.914	0.70	1.05	0.172	5.1
Mundaring (*MUN*)	0.051	G_2	NS	239.3	29,014	0.994	3.79	1.05	0.202	10.1
Scott Base (*SBA*)	0.198	G_1	EW	187.6	11,060	0.993	1.11	1.24	0.216	5.9
Chiengmai (*CHG*)	0.069	G_2	NS	293.1	29,115	0.995	3.81	1.09	0.228	5.6
Adelaide (*ADE*)	0.069	G_2	NS	229.3	30,810	0.996	4.29	1.15	0.271	10.2
Riverview (*RIV*)	0.168	G_2	NS	224.4	31,835	0.980	4.61	1.26	0.763	25.4
										Average: 7.8

(1) $\gamma_L(100) = 0.95 \cdot 10^{-4}$ km^{-1} for G_1 measured for Pacific Ocean paths (Mitchell et al., 1976); $\gamma_L(100) = 0.75 \cdot 10^{-4}$ km^{-1} for G_2 appropriate for mixed paths (Kovach, 1978).

(2) Sine or cosine of back azimuth depending on whether ground motion is NS or EW.

(3) Multiplication by $(a/10{,}000)^{1/2}$ where a is radius of the earth.

response of the layered medium, and χ = complex radiation pattern function. The source parameters present in the radiation pattern function are the dip angle δ and the slip angle λ; an important desired parameter, the seismic moment, enters simply as a scalar factor. For the calculation of the theoretical spectral amplitude, the oceanic model given by Harkrider (1970) was utilized inasmuch as the propagation path for G_1 was almost entirely oceanic (Fig. 8). The source depth was fixed at 6.5 km, the dip angle δ at 4°, and the slip angle λ at 90° (pure thrust). Selected G_1 and G_2 waves were Fourier analyzed, corrected for geometrical spreading and attenuation, and equalized to a distance of 90° (10,000 km) on a flat earth. Details of the spectral equalization are given in Table III. A period $T = 100$ s was chosen for the examination of the spectral amplitudes. For G_1 an attenuation coefficient $\gamma_L(100) = 0.95 \cdot 10^{-4}$ km^{-1} *observed* for Pacific Ocean paths (Mitchell et al., 1976) was used. Because of the mixed path for G_2 a value of $\gamma_L = 0.75 \cdot 10^{-4}$ km^{-1} was used (Kovach, 1978). Both G_1 and G_2 waves were utilized because it can be seen that the amplitude of the finiteness factor (Ben-Menahem, 1961) at a period of 100 s, $|\sin X/X|$ with:

$$X = \frac{\pi L}{T}\left(\frac{1}{V} - \frac{\cos\theta}{c}\right)$$

where L and V are the length and rupture velocity of the fault, is small in both the forward and backward quadrants for a fault length of only 50 km. The wavelength of G waves corresponding to a period of 100 s is about 450 km, much larger than the linear dimension (~50 km) of the source area of the Kalapana earthquake, as defined by the aftershock area (Tilling et al., 1976). Therefore, a step source-time function was assumed.

There are variations in the moment determinations, typical of seismic moment determinations, and we shall take the average of the surface wave values combined with the body-wave data for the estimate of the seismic moment of the Kalapana earthquake. This average value is $1.2 \cdot 10^{27}$ dyn cm.

The aftershock epicenter map by Tilling et al. (1976) shows an aftershock zone roughly 10 X 50 km. However, the aftershock zone, except for only two shocks, is confined to inland area and does not extend into the sea. The fact that a tsunami was generated offshore indicates that the source area of the earthquake was much larger than the area outlined by aftershocks. We have taken 2200 km^2 as being representative of the fault area of the Kalapana earthquake, a value consistent with P-wave, surface-wave and tsunami data. With a rigidity of $\mu = 3.9 \cdot 10^{11}$ dyn cm^2, and the relation $M = \mu A \bar{U}$, the average slip $\bar{U}$ along the fault plane is 1.4 m. This amount of slip is compatible with the amounts of horizontal offset observed across the Hilina fault system after the Kalapana earthquake (Tilling et al., 1976).

The 1.4-m slip on the shallow thrust plane produced a vertical movement on the more steeply dipping present sea floor of ~0.5 m, in agreement with the tsunami generation calculations of Hatori (1976) based on the observations of Loomis (1975) that suggest a vertical uplift of the sea floor of about 1 m. This inference, however, may easily be in error by a factor of 2 (H.G. Loomis, pers. comm. 1977).

From the above figures we can compute a stress drop $\Delta\sigma$ utilizing the empirical–theoretical relation between moment, fault area, and stress drop, namely (Kanamori and Anderson, 1975):

$$M = A^{3/2}(\Delta\sigma)\, C\,.$$

If we assume $\lambda = \mu$ for a dip slip fault, C, the nondimensional shape factor is ~1 leading to an inferred stress drop of 12 bar.

The computed stress drop of 12 bar is significantly less than the average value of 100 bar that has been suggested to be representative of intra-plate earthquakes.

5. Tsunami data

Hatori (1976) outlined the tsunami generation area of the earthquake by a ray-tracing method for tsunamis (Fig. 8) and obtained a generation area of 2200 km^2 that agrees with fault areas obtained by P-wave and surface-wave calculations. Hatori also obtained a sea-level elevation of 0.5–3 m as a result of uplift of the sea floor.

While uplift occurred at sea, subsidence was observed on land during the earthquake, and in the weeks following the earthquake subsidence continued. Total subsidence ranged from 0.8 to 3 m, depending upon the location (Tilling et al., 1976).

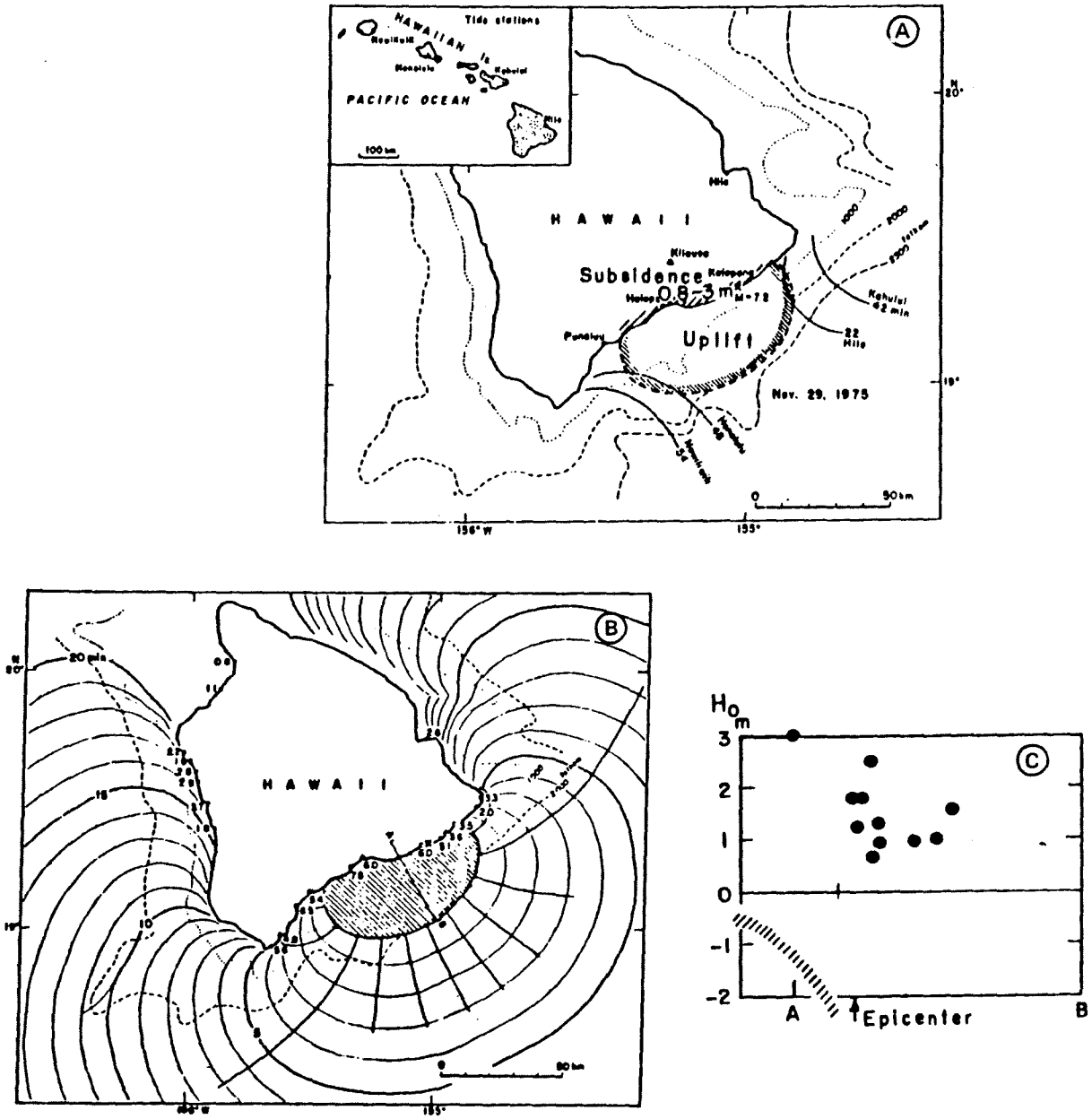

Fig. 8. The tsunami generating area for the Kalapana earthquake obtained by tsunami ray-tracing method by Hatori (1976).
A. Inverse refraction diagram to obtain generation area. Land subsidence data by Tilling et al. (1976).
B. Refraction diagram with inundation height provided by Loomis (1975).
C. Upper diagram shows profile of sea-level disturbance of source area (A–B) in figure B; lower is projection of subsidence profile.

A model of earthquake source mechanism, then, should account for uplift at sea and subsidence on land, and demarcation should coincide roughly with the coastline.

6. Interpretation

The preferred source mechanism solution is a low-angle overthrust across a fault plane with an updip

of 4° to the SE, plane L of Fig. 4. This fault plane corresponds to the ancient sea floor upon which the volcanic edifice of Kilauea was built. The geological structure as derived by various geophysical surveys (Broyles, 1977; Furumoto and Broyles, 1977) carried out in connection with a geothermal exploration program (Fig. 9).

The surface layer consists of subaerially extruded lava with P-wave velocity of 1.0 km/s above the water table and 2.5 km/s below the water table. Subaerially extruded lava is characterized by high porosity and permeability. Below the 2.5-km/s layer lava was found extruded under submarine conditions, having very low rock porosity and velocity of 3.0 km/s. Within the 3.0-km/s layer in a fractured region a commercially viable geothermal reservoir has been found. The reservoir is 18 km ENE of the earthquake epicenter, but it has been sketched into the model to show its position relative to the rest of the geological structure. A 5.25-km/s layer was found at a depth of 1.8 km. One property of the 5.25-km/s layer is that it is almost impermeable. To account for the data obtained by electrical resistivity surveys in the area, a resistivity of "infinity" must be positioned at depths of 1.9–2.2 km (Keller, 1973), the depths corresponding to the top of the 5.25-km/s layer.

Within the 5.25-km/s layer a dike complex was found with a P-wave velocity of 7.0 km/s and density in the range of 3.1 g/cm^3. The dike complex has been the passageway through which magma from the holding reservoir under the summit of Kilauea has worked its way down the east rift. Fiske and Jackson (1972) first proposed, and Swanson et al. (1976) have developed, a hypothesis of forceful intrusion of magma into the rift zone. According to this hypothesis, injection of magma under pressure laterally opens up vertical cracks, into which magma then works its way. The early magma movements occurred to the north, upon the flanks of Mauna Loa; subsequent incursions of magma occurred to the south, as the flank of Mauna Loa acted as an anchor to the north. The migration of magma passageways to the south has resulted in a broad dike complex, which in the Kalapana section amounts to 18 km (Broyles, 1977; Furumoto and Broyles, 1977).

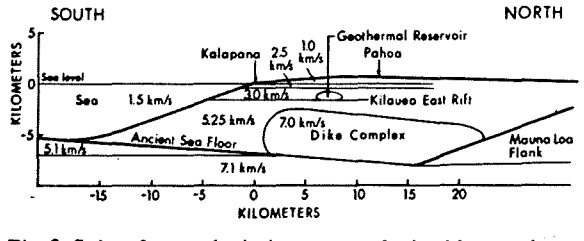

Fig. 9. Subsurface geological structure obtained by geophysical surveys of the Hawaii geothermal program. The numbers represent P-wave velocities. The 7.1-km/s layer was determined by Hill (1969).

Kilauea volcano has under its summit area a central vent through which magma from depths of 60 km has risen. Magma is then temporarily lodged in a central holding reservoir. The lava and magma in the rift zones have all come from the central holding reservoir. Hence, the volcanic edifice with its dike complex and associated extrusions sits on top of the ancient sea floor that existed before the volcano was formed. Mauna Loa volcano was formed earlier than Kilauea and parts of the Kilauea edifice rest on the flanks of Mauna Loa. Under the weight of the volcanic mass, the ancient sea floor has been downwarped. As there is little P-wave velocity contrast between the lowest layer of volcanic edifice and the first layer of oceanic crust, the ancient sea floor was not detected by seismic refraction, but by locations of microearthquakes. In a microearthquake survey, Suyenaga (1975) found a number of earthquakes distributed at 5-km depth throughout the region. The interpretation by Furumoto and Broyles (1977) was that these earthquakes delineated a discontinuity, and the only nearly horizontal discontinuity that could be postulated for the area is the ancient sea floor. The depth at which the ancient sea floor should exist coincided very well with the microearthquake data.

The Kalapana earthquake can be explained in the context of the hypotheses of the forceful intrusion of magma into the rift zone, and in turn the earthquake adds more information to the thermal process of the east rift. The intrusion of magma into the dike complex over the years has resulted in a steady buildup of pressure in the zone. Swanson et al. (1976) have tracked the buildup of stresses by means of geodetic surveys and were able to predict that an earthquake was imminent. At a certain stress level, slip or rupture occurred across the ancient sea floor, which could be the weakest interface in the region.

When the critical stress level was reached, the

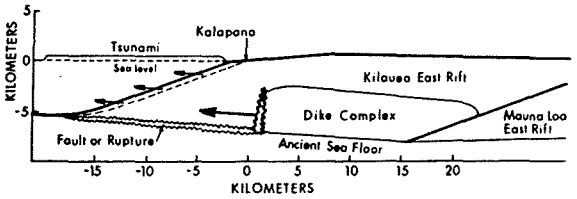

Fig. 10. The mechanism of the Kalapana earthquake and tsunami. The displacement of the island shelf and the upheaval of the sea surface have been exaggerated for illustrative purposes.

flank of Kilauea was pushed seaward over the ancient sea floor. It was an updip motion, an overthrust, because the ancient sea floor dipped under the island mass (Fig. 10). The sloping sea floor SE of Kalapana moved with the mountain mass, and because there was sufficient vertical component of displacement, the sea surface was uplifted 0.5–3 m. The uplifted sea surface then radiated in all directions as a tsunami.

The seaward fling of the mountain mass produced subterranean space along the SE margin of the dike complex. Adjustment to this disruption took the form of subsidence of the seashore along Kalapana in the weeks following the earthquake (Fig. 8).

One result of our analysis of the Kalapana earthquake was determination of the depth and dip of the ancient sea floor. Microearthquakes had first outlined the ancient sea floor, but because of the lack of resolution of focal depth determination, the best that could be said was that the ancient sea floor was located at a depth between 5 and 8 km (Furumoto and Broyles, 1977). The Kalapana earthquake occurred in the 7.1-km/s layer (cf. Fig. 3). The 7.1-km/s layer starts at a depth of 7 km (Hill, 1969), the same depth for the earthquake focus. We can say that the earthquake occurred at the top of the 7.1-km/s layer, at the SE margin of the dike complex. From the dip of nodal plane *L* (Fig. 5), we now know that the ancient sea floor dips under the island at 4°.

7. Conclusion

Analysis of P-wave data from teleseismic and local records showed that the Kalapana earthquake of 1975 was an overthrust along a fault plane with an updip of 4° to the SE, to seaward. The fault plane coincides with the ancient sea floor which pre-existed the volcano and upon which the volcanic edifice rests.

Body- and surface-wave data showed that the seismic moment was in the neighborhood of 10^{27} dyn cm and that the stress drop was on the order of tens of bars. This stress drop is relatively low compared with the "norm" for intra-plate earthquakes. The low values may have been due to the occurrence of the earthquake in a region of elevated temperatures. It will be interesting to examine whether other earthquakes that occur in areas of elevated temperatures such as geothermal areas exhibit characteristically low stress drops.

The updip displacement across the ancient sea floor of the island shelf was of sufficient vertical component to generate a tsunami. The subsidence of the land for weeks after the earthquake was an adjustment to the disruption in the subsurface structure.

The geological structure of the east rift obtained by a geothermal exploration program greatly helped in understanding the processes before, during, and after the earthquake. The hypothesis of forceful intrusion of lava into the rift zone and of the southward migration of magma passageways is consistent with observed data. The analysis of the earthquake, in turn, showed that the ancient sea floor was 7 km deep under Kalapana and that it dipped 4° under the island mass.

Acknowledgements

Robert L. Kovach thanks Gordon Eaton and Robert Koyanagi of the Hawaiian Volcano Observatory for the opportunity to examine seismograms of the local network on Hawaii.

Major support by this analysis was provided by the Hawaii Institute of Geophysics; the research was also supported by grants for geothermal research from ERDA E(04-3)-1093, and from U.S. Geological Survey Contracts 14-08-0001-15166 and 16721 at Stanford University.

References

Ando, M., 1976. A source model of the $M = 7.2$ Kalapana earthquake of November 29, 1975. EOS (Trans. Am.

Geophys. Union), 57: 954 (abstract).

Ben-Menahem, A., 1961. Radiation of seismic surface waves from finite moving sources. Bull. Seismol. Soc. Am., 51: 401–435.

Ben-Menahem, A. and Harkrider, D.G., 1964. Radiation patterns of seismic surface waves from buried dipolar point sources in a flat stratified earth. J. Geophys. Res., 69: 2605–2620.

Broyles, M., 1977. The structure of the east rift zone of Kilauea, Hawaii from seismic refraction, gravity and magnetic surveys. M. Thesis, University of Hawaii, Honolulu, Hawaii, 75 pp.

Fiske, R.S. and Jackson, E.D., 1972. Orientation and growth of Hawaiian volcanic rifts: The effect of regional structure and gravitational stresses. Proc. R. Soc. London, Ser. A, 329: 299–326.

Furumoto, A.S., 1976. A coordinated exploration program for geothermal sources on the island of Hawaii. Proc. Sec. U.N. Symp. on Development and Use of Geothermal Resources, 2: 993–1001.

Furumoto, A.S. and Broyles, M.L., 1977. Dimensions and thermal process of magma conduit underlying east rift zone of Kilauea volcano, Hawaii. Pap. presented at IASPEI/IAVCEI Joint Assem., Durham, Aug. 1977.

Hanks, T.C. and Wyss, M., 1972. The use of body-wave spectra in the determination of seismic-source parameters. Bull. Seismol. Soc. Am., 62: 561–589.

Harkrider, D., 1970. Surface waves in multilayered elastic media, Part II. Higher mode spectra and spectral ratios from point sources in plane layered earth models. Bull. Seismol. Soc. Am., 60: 1937–1987.

Hatori, T., 1976. Wave source of the Hawaii tsunami in 1975 and the tsunami behavior in Japan. J. Seismol. Soc. Jpn., Ser. 2, 29: 355–364.

Herrin, E., 1968. Seismological tables for P. Bull. Seismol. Soc. Am., 58: 1196–1219.

Hill, D., 1969. Crustal structure of the island of Hawaii from seismic refraction measurements. Bull. Seismol. Soc. Am., 59: 101–130.

Julian, B.R. and Anderson, D.L., 1968. Travel times, apparent velocities and amplitudes of body waves. Bull. Seismol. Soc. Am., 58: 339–366.

Kanamori, H. and Anderson, D.L., 1975. Theoretical basis of some empirical relations in seismology. Bull. Seismol. Soc. Am., 65: 1073–1095.

Keller, G.V., 1973. An Electrical Resistivity Survey of the Puna and Ka'u Districts, Hawaii County, Hawaii. Group Seven, Golden, Colo., 97 pp.

Keller, G.V., 1975. The Ophikao Prospects, Puna District. Microgeophysics Corp., Golden, Colo.

Kovach, R.L., 1978. Seismic surface waves and crustal and upper mantle structure. Rev. Geophys. Space Phys., 16: 1–13.

Loomis, H.G., 1975. The tsunami of November 29, 1975 in Hawaii. Hawaii Inst. Geophys., Rep. HIG-75-21, NOAA-JTRE 152, 29 pp.

Macdonald, G.A., 1956. Structure of Hawaiian volcanoes. Verh. Ned. Geol. Mijnbouwk. Genoot., 16: 1–22.

Mitchell, B.J., Leite, L.B.W., Yu, Y.K. and Herrmann, R.B., 1976. Attenuation of Love and Rayleigh waves across the Pacific at periods between 15 and 110 seconds. Bull. Seismol. Soc. Am., 66: 1189–1202.

Pho, H.T. and Behe, L., 1972. Extended distances and angles of incidence of P-waves. Bull. Seismol. Soc. Am., 62: 885–902.

Suyenaga, W., 1975. Results of the microearthquake survey and seismic studies of the Lower East Rift. Summ. Rep. Phase I, Hawaii Geothermal Proj., Univ. Hawaii, Honolulu, Hawaii, pp. 62–66.

Swanson, D.A., Duffield, W.A. and Fiske, R.S., 1976. Displacement of the south flank of Kilauea volcano: the result of forceful intrusion of magma into rift zones. U.S. Geol. Surv., Prof. Pap., 963, 39 pp.

Tilling, R.I., Koyanagi, R.Y., Lipman, P.W., Lockwood, J.P., Moore, J.G. and Swanson, D.A., 1976. Earthquake and related catastrophic events, island of Hawaii, Nov. 29, 1975 – A preliminary report. U.S. Geol. Surv. Circ., 140, 33 pp.

Kalapana quake 29 Nov 75
Rm 7.2 depth 7km